Development of Magneto-Thermo-Mechanical Analytical Models for High-Speed Induction Machine

L. Dahnoun[1,2], T. Lubin[1], N. Blet[3], J. Fontchastagner[1], R. Teggour[3], C. Viguier[2] and N. Takorabet[1]

[1]GREEN, Université de Lorraine, F-54000 Nancy, France.
[2]Electrical and Electronic Systems Research Group, Safran Tech, F-78114 Magny-Les-Hameaux, France.
[3]LEMTA, Université de Lorraine, F-54000 Nancy, France.

In the context of decarbonizing the transportation industry, there has been a steady increase in the amount of electrical power onboard, necessitating improvements in the performance of electrical machines to achieve higher specific powers. Additionally, due to the high demands placed on components, the magneto-thermo-mechanical properties of materials play a crucial role in the design of high-performance machines. This paper proposes an analytical procedure to address the three key physics involved in the design of a high-speed induction machine with a rotor composed of a copper layer. The electromagnetic models developed utilize a multi-harmonic approach based on the magnetic vector potential. For thermal analysis, the two-dimensional cylindrical steady-state heat equation is solved using the separation of variable technique. This method is chosen for its compatibility with further coupling with other physics, compared to the classic lumped-parameter approach. The mechanical model enables the study the stresses induced by centrifugal forces, employing a plane deformation approach. Finite element models are employed to validate the various developed models, ensuring their accuracy and reliability in predicting the performance of the high-speed induction machine.

***Key words*—Multiphysics, analytical model, potential vector formulation, steady-state heat equation, centrifugal effects.**

I. Introduction

ASYNCHRONOUS operation at elevated speeds introduces complexities that manifest as increased electromagnetic, thermal, and mechanical stresses, consequently affecting motor performance and reliability [1]. Traditional design methodologies typically rely on either empirical techniques or computationally intensive finite element analysis (FEA), both of which pose significant time and resource burdens. For instance, FEA simulations may require hours to days to complete and demand hundreds of gigabits of computational resources [2].

In contrast, optimization-driven design necessitates rapid (few seconds) and precise (less than 10% of error) analytical models. The ones based on equivalent circuit representations offer expedited insights into motor behavior, although they often involve approximations in parameter evaluation. To address this limitation, a shift towards field-based modeling has emerged, leveraging solutions to Laplace's equation for efficient computation of critical parameters such as torque and rotor branch impedance [3].

Furthermore, the integration of analogous thermal [4] and mechanical [5] considerations enables the development of a comprehensive multiphysics model. The paper's value proposition is to develop those approach in each physic adapting them to high-speed (above 180m/s of tip speed) on a simplified geometry application.

II. Electromagnetic Model of the High-Speed Induction Machine (HSIM)

The objective of this part is to develop an electromagnetic model for the structure presented in Fig. 1 composed of a classical stator winding and a rotor cage composed by an homogeneous copper ring and a ferromagnetic yoke.

The resolution method developed below consists of a magneto-harmonic study that allows to account for the currents induced in the different layers of the rotor. The objective is to identify the shape of the magnetic vector potential by solving the Poisson and Laplace equation in each layer of the model. The study is not limited to the fundamental but considers all the space phase belt harmonics symbolized by the index n. Only linear behavior of ferromagnetic parts are considered.

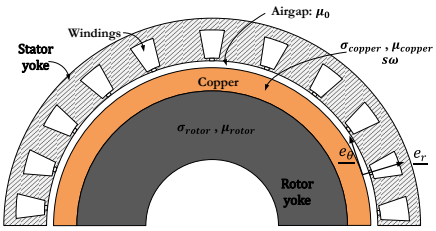

Fig. 1. Cross-section of the studied high-speed induction machine.

A. *Stator winding modelling*

As for the stator current density, it is necessary to implement a spectral decomposition of the currents consisting in separating the contribution of each sources generating specific harmonics in the winding.

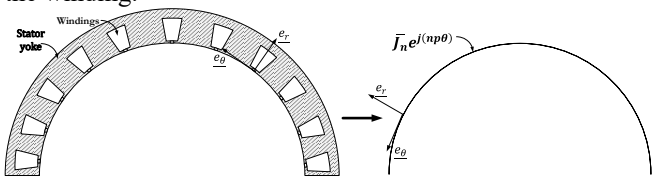

Fig. 2. Modeling of stator winding.

The use of the Discrete Fourier Transform (DFT) on slots' currents (with p the pole pairs) makes it possible to analyze the spectrum of equivalent linear current density reported to the airgap bore radius (Fig. 2). Thus, from the winding matrix as well as the sinusoidal currents injected to the stator it is possible to trace the current density spectrum.

On the left of Fig. 3 it can be seen that depending on the angular position, the current seen from the stator can be null if directly facing a tooth or non-null if facing a slot. This switch allows to decompose the resulting signal in a sum of harmonics. On the right of Fig. 3, the importance of different harmonics on the signal can be read. For example, in the presented case, it is possible to identify teeth harmonics (-23 and 25) as the decomposition result from 24 slots winding matrix. It is also possible to identify the others classical harmonics of rank $1 \pm 6k$ with k an integer. The sign of the harmonics allows to identify either the resulting electromagnetic wave turn in a direct or indirect way.

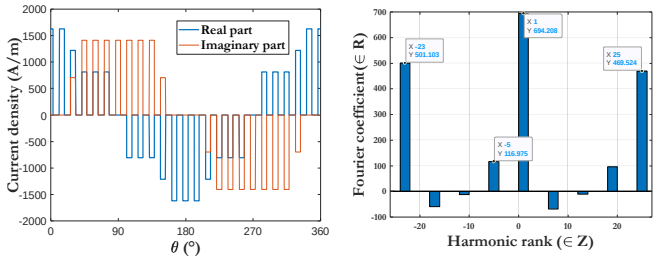

Fig. 3. Decomposition of the linear density of currents at the stator.

B. Potential vector formulation

A "subdomain method" constitutes an efficient tool to evaluate the magnetic field distribution in electrical machine and can be applied for different geometries/types of machines [3].

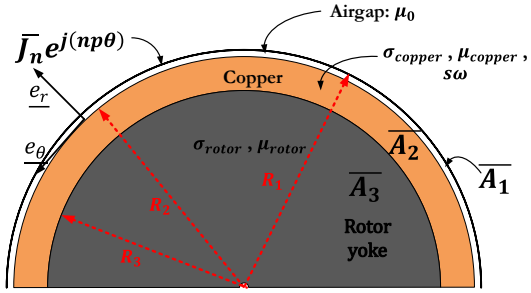

Fig. 4. Three-layer equivalent model of the machine.

In the copper and rotor yoke, the equation to solve is (1), in the air gap it is (2) and the form of the solutions, issued from the conservation on the tangential part of the flux density and the continuity of the potential vector, are (3).

$$\frac{\partial^2 \overline{A_n}}{\partial r^2} + \frac{1}{r}\frac{\partial \overline{A_n}}{\partial r} + \frac{1}{r^2}\frac{\partial^2 \overline{A_n}}{\partial \theta^2} = j\mu\sigma\omega_{rn}\overline{A_n} \quad (1)$$

$$\frac{\partial^2 \overline{A_n}}{\partial r^2} + \frac{1}{r}\frac{\partial \overline{A_n}}{\partial r} + \frac{1}{r^2}\frac{\partial^2 \overline{A_n}}{\partial \theta^2} = 0 \quad (2)$$

$$\begin{aligned} A_1(r,\theta) &= \sum_{k\geq 1}\left(C_5 r^k + C_6 r^{-k}\right)\left(C_7 e^{jk\theta} + C_8 e^{-jk\theta}\right) \\ A_2(r,\theta) &= \sum_{k\geq 1}\left(C_1 J_k(\lambda_{2,k} r) + C_2 Y_k(\lambda_{2,k} r)\right)\left(C_3 e^{jk\theta} + C_4 e^{-jk\theta}\right) \\ A_3(r,\theta) &= \sum_{k\geq 1}\left(C_9 J_k(\lambda_{3,k} r)\right)\left(C_{10} e^{jk\theta} + C_{11} e^{-jk\theta}\right) \end{aligned} \quad (3)$$

with: μ the magnetic permeability,
σ the electrical conductivity,
C_n unknown coefficients,
$\lambda_{n,k} = -j\mu\sigma\omega_{rn} = -j\mu\sigma[(1-(1-g)n)\omega_s]$.

However, because of high-speed, the model considering 3 layers diverges when studying high-frequencies (Fig. 4). Thus, two other models one considering only the airgap by setting the right current density corresponding to skin depth of the copper layer and another with only airgap and copper layer are developed (Fig. 5).

By doing this, in the case of the three-layer model the identification of the unknows issues from the resolution of the system (4):

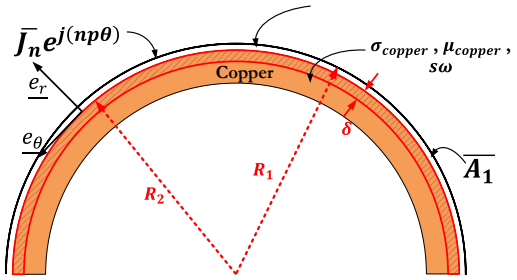

Fig. 5. One-layer model of the machine using skin depth impedance.

$$MX = B \quad (4)$$

with: X the vector with the unknown coefficient,
$B = [\bar{J}_n \quad 0 \quad 0 \quad 0 \quad 0]^T$,

$$M = \begin{bmatrix} -dR_1^{np-1} & dR_1^{-(np+1)} & 0 & 0 & 0 \\ R_2^{np} & R_2^{-np} & -J_{np}(\lambda_{2,np}R_2) & -Y_{np}(\lambda_{2,np}R_2) & 0 \\ dR_2{}^{np-1} & -dR_2^{-(np+1)} & aJ'_{np}(\lambda_{2,np}R_2) & aY'_{np}(\lambda_{2,np}R_2) & 0 \\ 0 & 0 & J_{np}(\lambda_{2,np}R_3) & Y_{np}(\lambda_{3,np}R_3) & -J_{np}(\lambda_{3,np}R_3) \\ 0 & 0 & bJ'_{np}(\lambda_{2,np}R_3) & bY'_{np}(\lambda_{2,np}R_3) & cJ'_{np}(\lambda_{3,np}R_3) \end{bmatrix}$$

where $a = -\frac{1}{\mu_{copper}}\lambda_{2,np} | b = \frac{1}{\mu_{copper}}\lambda_{2,np} | c = -\frac{1}{\mu_{rotor}}\lambda_{3,np} | d = \frac{1}{\mu_0}np$,

Whereas in the one-layer model:

$$M = \begin{bmatrix} -\frac{1}{\mu_0}npR_1{}^{np-1} & \frac{1}{\mu_0}npR_1{}^{-(np+1)} \\ npR_2{}^{np-1} - \frac{1+j}{\delta}R_2{}^{np} & -npR_2{}^{-(np+1)} - \frac{1+j}{\delta}R_2{}^{np} \end{bmatrix}$$

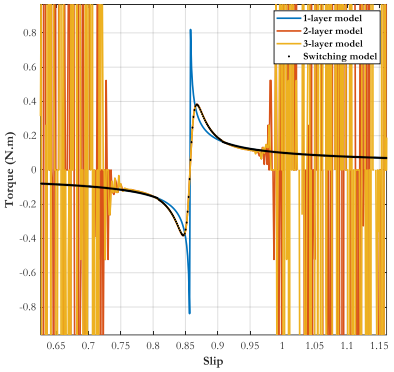

Fig. 6. Torque due to the harmonic 7 obtained with the three different models.

The torque calculated far from the natural frequency associated with the harmonic (slip=0.85) diverges with the three and two-layer models as it corresponds to high frequencies regions. Whereas around 0.85, it is the opposite with the one-layer model which begins to diverge (Fig. 6). Switch between the model can be related to a value of skin depth in a first approximation. However, this method does not allow to have a

generic sizing model as if the geometry is changed, the value of the skin depth at which the different models gives the same results will also change. Thus, a condition on the matrix conditioning is done allowing to have better results for a wide range of HSIM.

The developed model is validated thanks to FE done with FEMM software, and a deviation of 10% is observed on the value of the maximum torque. The actual analytical model considers a constant current alimentation in the stator (Fig. 7). Future version of this work will include a voltage supply so that the stator current will depend on the slip.

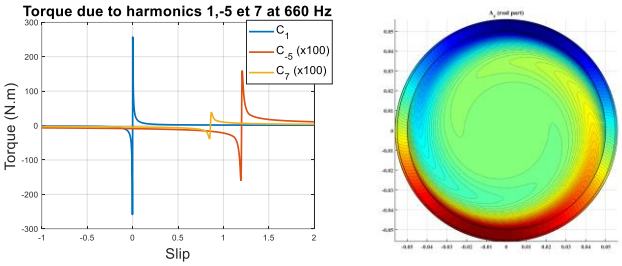

Fig. 7. Torque for the 3 first harmonics (left) and potential vector for the 1st harmonic and p=1 (right) obtained with developed models.

III. THERMAL MODEL OF THE HSIM

When designing a high-speed induction machine, thermal management aspects are crucial to ensure the integrity of the machine. In this study a focus on analytic models is done. The most commonly and widely used is based on a lumped-parameter scheme that consider an electro-thermal equivalence to evaluate the temperature in the different regions of the machine. Besides the fact that this mean is easily applicable, its accuracy depends on the discretization and the number of elements considered. Moreover, in the scope of implementing the coupling between the other analytical models to provide a multi-physical sizing tool, this way is not the best. Thus, resolution of partial differential equation governed by the steady state heat equation (5) is done. As the studied system is perfectly axisymmetric and assuming that the materials properties are set anisotropic, a two-dimensional model is sufficient.

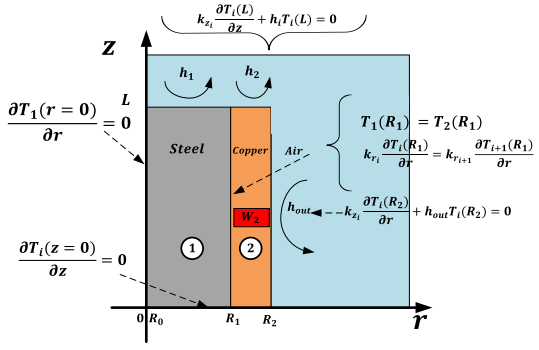

Fig. 8. Two-layer thermal model of the rotor.

A first version of the model considers only the rotor of the machine thanks to a two-layers cylinder within which the external layer has a constant volumetric heat source representing the copper layer at the rotor. The heat equation of the system for a layer i with volumetric heat source W_2 (W.m^{-3}) is:

$$\frac{k_{r_i}}{r}\frac{\partial}{\partial r}\left(r\frac{\partial T_i}{\partial r}\right)+k_{z_i}\frac{\partial^2 T_i}{\partial z^2}+\mathrm{W}_2=0 \qquad (5)$$

With: k_{r_i} and k_{z_i} the thermal conductivities of the layer i in respectively the radial and axial directions (W.m^{-1}.K^{-1}).

The same equation without the volumetric heat source term is solved in the first layer. In a non-exhaustive review of literature, ways to solve multi-layer heat conduction problems consists in Laplace transform method [4], Green's function approach, orthogonal expansion technique [6], finite integral transform technique and separation of variable method. The latter method does not appear to have been applied to steady state problem with inhomogeneous boundary conditions in intermediary layers.

To completely define the model, boundary conditions representing the convection on the external surface of the rotor and on its fore and back end are included with different values of convective coefficient depending of the layer considered as shown in Fig. 8. Symmetries following r and z are included too. The expression of the solution in each layer after implementing the separation of the variables in the resolution of the partial differential equation consist in Fourier series with modified Bessel functions following r and cosinus following z:

$$\begin{cases} T_1(r,z)=\sum_{n=1}^{N} A_n \mathrm{I}_0\left(\frac{\alpha_n}{\sqrt{k_{r_1}/k_{z_1}}}r\right)\cos(\alpha_n z) \\ T_2(r,z)=\sum_{k=1}^{K}\left\{B_k \mathrm{I}_0\left(\frac{\beta_k}{\sqrt{k_{r_2}/k_{z_2}}}r\right)+C_k \mathrm{K}_0\left(\frac{\beta_k}{\sqrt{k_{r_2}/k_{z_2}}}r\right)+\mathrm{K}_k\right\}\cos(\beta_k z) \end{cases}$$

with: α_n the eigenvalues of the first layer satisfying the transcendental equation: $\alpha_n=\frac{h_1}{k_{z_1}}\mathrm{cotan}(\alpha_n L)$,

β_k the eigenvalues of the second layer satisfying the transcendental equation : $\beta_k=\frac{h_2}{k_{z_2}}\mathrm{cotan}(\beta_k L)$,

$\mathrm{K}_k=\frac{4W_2\sin(\beta_k L)}{k_{z_2}\beta_k{}^2(2\beta_k L+\sin(\beta_k L))}$ the term due to volumetric heat source found by decomposition on the eigenfunctions base of the problem.

For the validation of the developed model, FEMM software is used which allows to simulate the same parameters as it can be launched from Matlab. The two-layers model is simulated with the following parameters (Table I):

TABLE I
PARAMETERS OF THE TWO-LAYER MODEL.

External temperature (°C)	25
Geometry (m)	$R_1=0.1$ $R_2=0.12$ $L=0.125$
Convective heat transfer coefficient (W.m^{-2}.K^{-1})	$h_1=h_2=100$
Convective heat transfer coefficient with external layer (W.m^{-2}.K^{-1})	$h_{out}=100$
Thermal conductivity in radial direction (W.m^{-1}.K^{-1})	$k_{r_1}=49.8$ $k_{r_2}=401$
Thermal conductivity in axial direction (W.m^{-1}.K^{-1})	$k_{z_1}=4.98$ $k_{z_2}=401$
Volumetric heat source (W.m^{-3})	$\mathrm{W}_2=1.4.10^6$

It can clearly be seen from Fig. 9 that the results from the analytical model are exactly the same as the finite element one in the majority of regions. The layer with a uniform volumetric heat source is at the highest temperature. A little drop at the fore and back end of this layer is due to the convective exchange. This is also observed in the first layer with a more significant drop when moving away from the heated layer.

By zooming at the interface region between the two layers at fore and back end, it can be observed a concentration of little high deviation than in the all geometry (Fig. 10). This is due to the presence of multiple boundary conditions in this region (strong convective effects and solid layer change). These peaks of deviation can be reduced by increasing the number of eigenvalues used in the decomposition of the temperature in each region as shown in Table II.

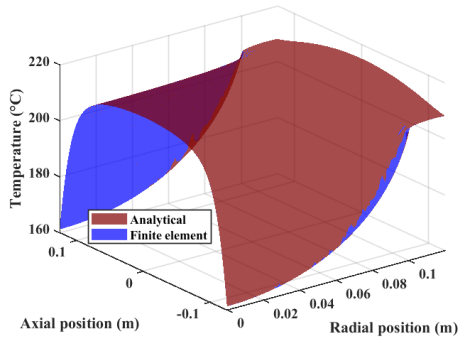

Fig. 9. Temperature distribution issued from the two-layers models

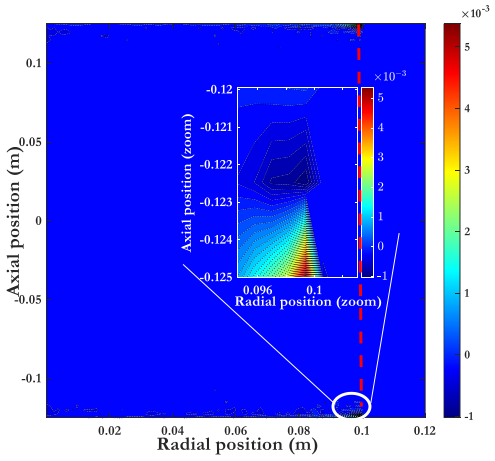

Fig. 10. Heatmap of the deviation between FE and analytical model.

TABLE II
IMPACT OF THE NUMBER OF EIGENVALUES ON THE RESULTS.

Number of eigenvalues	CPU time analytical model (s)	CPU time FE model (s)	Relative deviation range (%)	Average deviation (%)
5	0.195	3	[-3.5;8]	0.49
10	0.20	3	[-1.5;3.7]	0.127
20	0.20	3	[-0.6;1.6]	0.035
30	0.215	3	[-0.4;1.0]	0.019
40	0.218	3	[-0.3;0.7]	0.013
50	0.26	3	[-0.1;0.5]	0.011

Moreover, the higher is this number, the smaller is the relative deviation range and average deviation. In all the cases this approaches indicates very accurate results and is more than ten times quicker than finite element models.

A second version of the model considers a five-layers cylinder within which two of them has a constant volumetric heat source representing the stator windings and the copper layer of the rotor.

In order to consider the airgap layer, an equivalent thermal conductivity coefficient is used in the radial direction. This coefficient in the radial direction is directly related to the speed of the rotor and the nature of the flow in the airgap. Its value in the axial direction is supposed to be equal to the one in normal conditions at 293 K ($k_{z_3} = 0.024$ W.m^{-1}.K^{-1}) by making the assumption that the airflow is the same in the length of the airgap. To extrapolate the values of this coefficient in the radial direction, finite element simulations were done with Ansys for 3 different airgaps and different speeds of the rotor (Fig. 11).

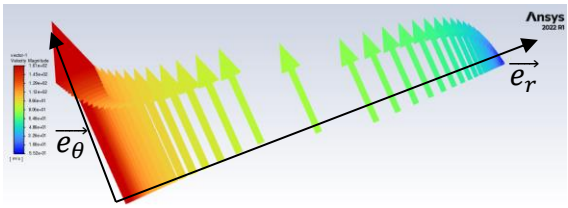

Fig. 11. Evolution of speed vector in the airgap.

The distribution of the speed vector in the airgap highlights that the equivalent conductivity in the radial direction will change.

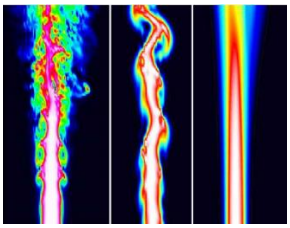

Fig. 12. Turbulent jet prediction (DNS left, LEF middle and RANS right) [5].

The Reynolds-Averaged Navier-Stokes (RANS) equations are a set of equations used to describe the motion of fluid flow in engineering applications. They are augmented with turbulence models to predict turbulent flow behavior. However, for highly turbulent flows characterized by complex structures and unsteady phenomena, RANS models may not capture the full range of turbulence effects. Large Eddy Simulation (LES) and Direct Numerical Simulation (DNS) offer alternatives (Fig. 12). DNS resolves all turbulent scales, making it computationally expensive for practical applications. LES, on the other hand, filters out small scales and resolves larger ones, reducing computational costs [8]. In the present case the RANS approach is done regarding the degree of precision needed. Moreover, among the various turbulence models used in RANS simulations, the k−ω model is chosen as it offers distinct advantages over the traditional k−ϵ model in capturing turbulence behavior near walls and in adverse pressure gradient flows. Thus, the FE model consist in a ring representing the airgap, with a moving surface for the rotor and a static surface for the stator with ΔT the temperature difference between the

two surfaces.

To determine the equivalent thermal conductivity k_{eq}, conservation of the heat flux q within the inner radius of the airgap is used (Fig. 13) as following:

$$-k_{eq}\frac{\Delta T}{e_{gap}} = h\Delta T = q \tag{6}$$

The results shown in Fig. 14 allows to identify the temperature distribution in the electrical machine with an average deviation with FE model of 0.5%.

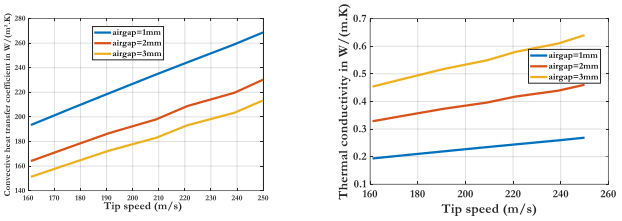

Fig. 13. Results from FE model of the airgap.

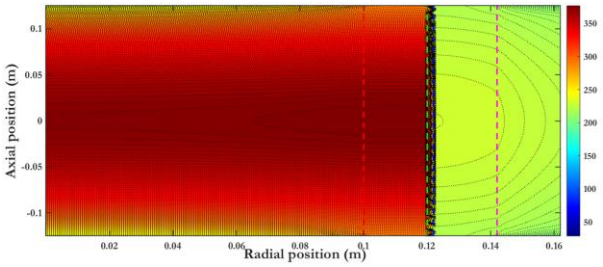

Fig. 14. Heatmap from analytical five-layers model of a random topology with airgap properties issued from extrapolation of Ansys results.

IV. Mechanical Model of the HSIM

Different methodologies in continuous media mechanics leads to the evaluation of the stresses in a rotor caused by the centrifugal effects [5]. For high-speed rotor, the most suitable is the displacement method as the rotating part is more likely to be a long axially extended cylinder. This approach assume that the displacement field is 2D (only r and θ dependency) leading to a 3D stress tensor. Thus, the axial constraints which cannot be neglected in this type of rotor is considered. Then fundamental principle of the dynamics is applied and lead to a partial differential equation:

$$div(\underline{\sigma}) + \rho \underline{f} = 0 \tag{7}$$

$$\frac{\partial^2 u_r}{\partial r^2} + \frac{1}{r}\frac{\partial}{\partial r}(u_r) - \frac{u_r}{r^2} = -\frac{\rho\omega^2}{\lambda+2\mu}r \tag{8}$$

$$\begin{cases} u_r^k(r) = -\dfrac{\rho\omega^2}{8(\lambda+2\mu)}r^3 + {K_1}^k r + \dfrac{{K_2}^k}{r} \\ \sigma_{rr}^k = -\dfrac{\rho\omega^2}{8(\lambda+2\mu)}r^2(4\lambda+6\mu) + {K_1}^k(2\lambda+2\mu) - \dfrac{{K_2}^k}{r^2}2\mu \end{cases} \tag{9}$$

with: $\underline{u}$ the displacement field,
λ, μ, Lamé's coefficients,
ρ the density,
${K_1}^k$ and ${K_2}^k$ are unknown coefficients for each of the N layers,
ω the rotational speed,
$\underline{f}$ volumic forces induced by the rotational speed, $\underline{f} = r\omega^2\underline{e_r}$.

Then boundary conditions have to be chosen to account for the different expansions of the material of each layer due to the respective mechanical properties (Fig. 15). This will impact the condition of continuity of the displacement at the interface between the N layers.

$$\begin{aligned} &\sigma_{r_N}(R_{ext_N}) = 0 \\ &\sigma_{r_k}(R_{ext_k}) = \sigma_{r_{k+1}}(R_{int_{k+1}}) && k=1...N-1 \\ &R_{ext_k} + u_{r_k}(R_{ext_k}) = R_{int_{k+1}} + u_{r_{k+1}}(R_{int_{k+1}}) && k=1...N-1 \\ &u_{r_1}(0) \neq \infty \end{aligned} \tag{10}$$

Simulating the same five-layer rotor with the developed model and a finite element software allows the validation of the analytical model.

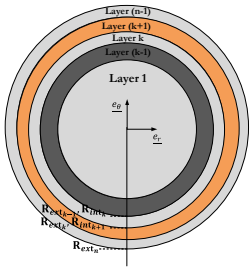

Fig. 15.Schematic representation of a multilayered rotor.

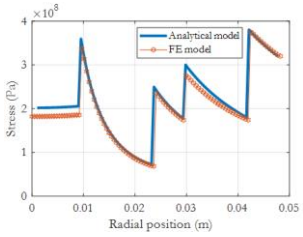

Fig. 16.Von Misses stress in a 5-layer rotor at high speed (40 krpm).

The results shown on Fig. 16 allow to validate the analytical model as the maximum deviation with FE results is of 3%. At each new layer, a peak of constraint is resulting from the different properties of the matter and from the force fit at the interface to provide mechanical handling between the layers at high-speeds.

V. Conclusion

The utilization of the three developed electromagnetic models, contingent upon the operational speed, facilitates a precise estimation of the output performance of high-speed induction machines across a broad speed spectrum. The thermal and mechanical analytical models yield highly accurate (less than 10% of deviation) and rapid results (few seconds). A specialized methodology has been devised for the airgap layer, enabling the determination of an equivalent thermal conductivity that accounts for turbulent flow effects within this region. Incorporating temperature-dependent material properties allows for the examination of temperature's influence on both mechanical and magnetic characteristics. Given the uniformity of the overall approach, seamless coupling between the three physics can readily be achieved in further version of this work.

References

[1] Pyrhönen, J., Nerg, J., Mikkola, A., Sopanen, J., & Aho, T. (2009). Electromagnetic and mechanical design aspects of a high-speed solid-rotor induction machine with no separate copper electric circuit in the megawatt range. Electrical engineering, 91(1), 35-49.

[2] Gerada, D., Mebarki, A., Brown, N. L., Bradley, K. J., & Gerada, C. (2010). Design aspects of high-speed high-power-density laminated-rotor induction machines. IEEE Transactions on Industrial Electronics, 58(9), 4039-4047.

[3] Lubin, T., S. Mezani, and A. Rezzoug. "2-D Exact Analytical Model for Surface-Mounted Permanent-Magnet Motors With Semi-Closed Slots." In: IEEE Transactions on Magnetics 47.2, pp. 479–492. doi: 10.1109/TMAG.2010.2095874.

[4] X. Lu, P. Tervola and M. Viljanen, "A new analytical method to solve the heat equation for a multi-dimensional composite slab" in J. Phys. A: Math. Gen. 38, 2005, 2873-2890.

[5] L. Dahnoun et al., 'Comparison Of Methods For Evaluating Mechanical Stress In The Rotor Of High-Speed Machines', in 2022 International Conference on Electrical Machines (ICEM), Sep. 2022, pp. 752–759. doi: 10.1109/ICEM51905.2022.9910837.

[6] C. W. Tittle "Boundary value problems in composite media: quasi-orthogonal functions" in Journal of Applied Physics, 1965, vol. 36, no 4, p. 1486-1488.

[7] A. Maries, A. Haque, S. L. Yilmaz, M. B. Nik, and G. E. Marai, ‘Interactive Exploration of Stress Tensors Used in Computational Turbulent Combustion’, in New Developments in the Visualization and Processing of Tensor Fields, D. H. Laidlaw and A. Vilanova, Eds., in Mathematics and Visualization. , Berlin, Heidelberg: Springer Berlin Heidelberg, 2012, pp. 137–156. doi: 10.1007/978-3-642-27343-8_7.

[8] P. Sagaut and Y.-T. Lee, ‘Large Eddy Simulation for Incompressible Flows: An Introduction. Scientific Computation Series’, Applied Mechanics Reviews, vol. 55, p. 115, Nov. 2002, doi: 10.1115/1.1508154.